nature nanotechnology

LETTERS

https://doi.org/10.1038/s41565-019-0402-5

Coulomb blockade in an atomically thin quantum dot coupled to a tunable Fermi reservoir

Mauro Brotons-Gisbert[1*], Artur Branny[1,4], Santosh Kumar[1,5], Raphaël Picard[1], Raphaël Proux[1], Mason Gray[2], Kenneth S. Burch[2], Kenji Watanabe[3], Takashi Taniguchi[3] and Brian D. Gerardot[1*]

Gate-tunable quantum-mechanical tunnelling of particles between a quantum confined state and a nearby Fermi reservoir of delocalized states has underpinned many advances in spintronics and solid-state quantum optics. The prototypical example is a semiconductor quantum dot separated from a gated contact by a tunnel barrier. This enables Coulomb blockade, the phenomenon whereby electrons or holes can be loaded one-by-one into a quantum dot[1,2]. Depending on the tunnel-coupling strength[3,4], this capability facilitates single spin quantum bits[1,2,5] or coherent many-body interactions between the confined spin and the Fermi reservoir[6,7]. Van der Waals (vdW) heterostructures, in which a wide range of unique atomic layers can easily be combined, offer novel prospects to engineer coherent quantum confined spins[8,9], tunnel barriers down to the atomic limit[10] or a Fermi reservoir beyond the conventional flat density of states[11]. However, gate-control of vdW nanostructures[12–16] at the single particle level is needed to unlock their potential. Here we report Coulomb blockade in a vdW heterostructure consisting of a transition metal dichalcogenide quantum dot coupled to a graphene contact through an atomically thin hexagonal boron nitride (hBN) tunnel barrier. Thanks to a tunable Fermi reservoir, we can deterministically load either a single electron or a single hole into the quantum dot. We observe hybrid excitons, composed of localized quantum dot states and delocalized continuum states, arising from ultra-strong spin-conserving tunnel coupling through the atomically thin tunnel barrier. Probing the charged excitons in applied magnetic fields, we observe large gyromagnetic ratios (~8). Our results establish a foundation for engineering next-generation devices to investigate either novel regimes of Kondo physics or isolated quantum bits in a vdW heterostructure platform.

Our device, shown schematically in Fig. 1a, consists of a quantum dot in monolayer WSe_2 separated from a Fermi reservoir in few-layer graphene by a monolayer hBN tunnel barrier. The WSe_2 is fully encapsulated on the bottom side by hBN (see Supplementary Fig. 1). This heterostructure was mechanically stacked in an inert environment on an insulating SiO_2 layer on a n-doped Si substrate (back gate). Gate-tuning is achieved by applying a bias V_g between the graphene electrode and the grounded back gate. Confocal photoluminescence imaging of the sample at a temperature of 3.8 K and $V_g = 0$ V reveals a few localized spots with higher photoluminescence intensity than the homogeneous background photoluminescence (Fig. 1b). The localized bright spots show discrete spectrally narrow peaks arising from WSe_2 quantum emitters[14–16] that are spectrally and spatially isolated due to local strain[17–20]. Here, local strain is provided from a wrinkle in the bottom hBN layer (Supplementary Fig. 1). Figure 1c shows V_g-dependent photoluminescence spectra measured at the brightest spot in Fig. 1b. Near $V_g = 0$ V, we observe three spectrally narrow lines corresponding to the neutral excitons (X^0) of three different optically active quantum dots (labelled A to C). Notably, the neutral exciton energy of dots A, B and C is independent of the vertical electric field across the device, demonstrating minimal quantum confined Stark effect for these WSe_2 quantum dots, in contrast to previous reports for WSe_2 quantum dots[21] but similar to two-dimensional excitons in TMDs[22]. At $V_g \approx -7$ V (dot A) and $V_g \approx -13$ V (dots B and C), the emission energy changes abruptly as a second electron overcomes the electron–electron Coulomb energy (U_{ee}) and tunnels into the quantum dot (schematically represented in the top part of Fig. 1d), creating negatively charged excitons (X^{1-}) with binding energies of ~25 meV (dot A) and ~23 meV (dots B and C). Additionally, for dot B we observe a spectral jump at $V_g > 10$ V as a second hole overcomes the hole–hole Coulomb energy (U_{hh}) and tunnels into the quantum dot (schematically represented in the bottom of Fig. 1d) to create the positively charged exciton (X^{1+}) with 7 meV binding energy. These results demonstrate an unambiguous Coulomb blockade at the single particle level and the unique ability to tune the Fermi reservoir from n-type to p-type in a vdW heterostructure.

To elucidate the nature of WSe_2 quantum dots, their strong tunnel coupling to the tunable Fermi reservoir and the consequences on the excitonic states, we focus in detail on dot B, which exhibits both the X^{1-} and X^{1+} at reasonably modest V_g. Figure 2a shows V_g-dependent high-resolution photoluminescence spectra. At $V_g = 0$ V, the X^0 exhibits a doublet split by ~830 μeV with orthogonally linear polarized emission (see Supplementary Fig. 4). Conversely, for X^{1-} and X^{1+} (at $V_g < -9$ V and $V_g > 16$ V, respectively) we observe a single spectral line, in contrast to a previous report[23]. The inset in Fig. 2a shows a diagram representing the exciton states. For X^0, the doublet is a fine-structure splitting (FSS) arising due to electron–hole exchange interaction energy (Δ_{FSS}), commonly observed for neutral excitons in InAs/GaAs[2,24] or WSe_2 (refs. [14–17]) quantum dots. On adding a second electron or hole to the neutral exciton, the minority particle interacts with a spin singlet and the exchange interaction vanishes. Notably, the exchange interaction only disappears in charged excitons for quantum dots in the strong confinement regime[24], identifying the nature of the monolayer WSe_2 quantum dots.

Numerous signatures of the strong coupling regime between both electrons and holes in the quantum dot and the graphene Fermi

[1]Institute of Photonics and Quantum Sciences, SUPA, Heriot-Watt University, Edinburgh, UK. [2]Boston College Department of Physics, Chestnut Hill, MA, USA. [3]National Institute for Materials Science, Tsukuba, Japan. [4]Present address: Department of Applied Physics, Royal Institute of Technology, Stockholm, Sweden. [5]Present address: Indian Institute of Technology, Goa GEC Campus, Ponda, Goa, India. *e-mail: M.Brotons_i_Gisbert@hw.ac.uk; B.D.Gerardot@hw.ac.uk

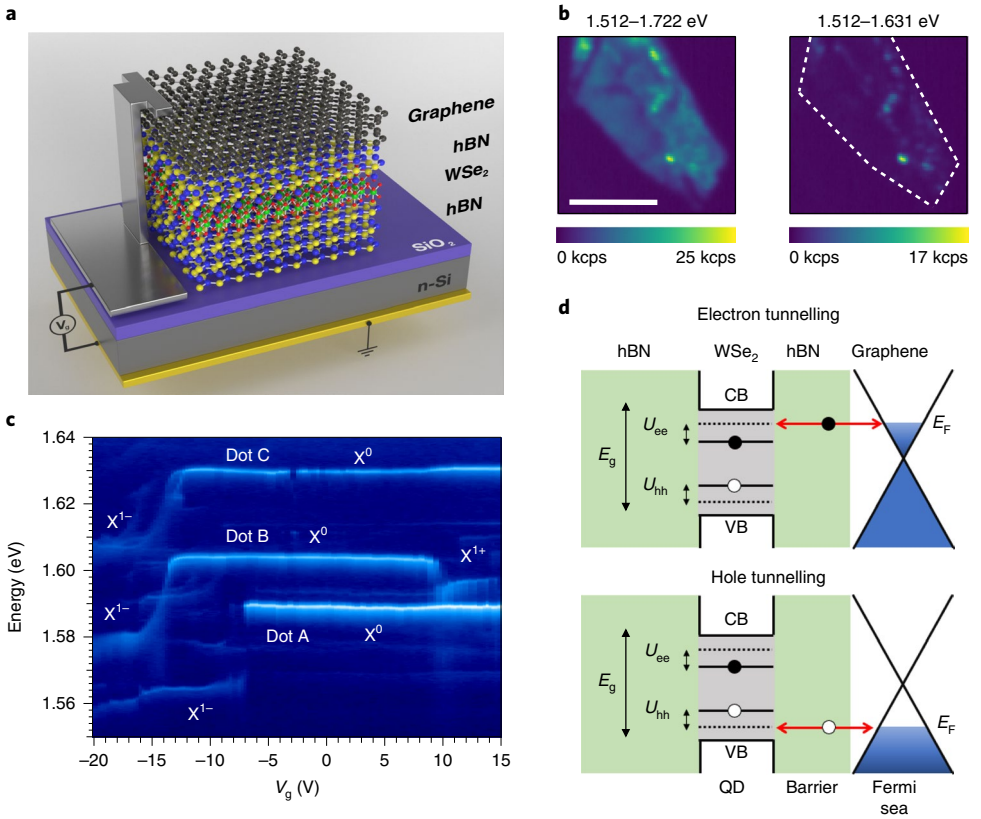

Fig. 1 | Coulomb blockade in a vdW heterostructure device. a, Sketch of the vdW charge-tunable quantum dot device. **b**, Colour-coded spatial map of the integrated photoluminescence signal of the WSe_2 in the spectral range of 1.512–1.722 eV (left) and 1.512–1.631 eV (right), highlighting the full flake and the single quantum emitters, respectively. The localized bright spots in the right panel correspond to quantum dots. The white dashed line indicates the edges of the WSe_2 monolayer region. kcps, kilo counts per second. Scale bar, 10 μm. **c**, Voltage-dependent low-resolution photoluminescence of three quantum dots at the brightest spot in **b** showing neutral (X^0), negatively charged (X^{1-}) and positively charged (X^{1+}) exciton species and Coulomb blockade. The unlabelled spectral features with weak peak intensity in **c** originate from distinct quantum dots unrelated to dots A, B and C (see Supplementary Information). **d**, Schematic representation of the electron (filled circles) and hole (open circles) tunnelling through the hBN barrier from the Fermi reservoir in the graphene to the quantum dots in WSe_2. CB, VB and E_g represent the conduction band, valence band and the energy bandgap of the WSe_2 quantum dots, respectively. U_{ee} (U_{hh}) represents the electron–electron (hole–hole) Coulomb interaction energy. QD, quantum dot.

reservoir can be found in the V_g-dependent photoluminescence spectra. First, the charging steps are abrupt in voltage, indicating the tunnelling rate is much faster than exciton recombination rate (~1–10 ns for WSe_2 quantum dots[14–17]). Second, the energies of the X^0 doublet peaks redshift near the edges of the plateau, indicating hybridization of energy levels in the quantum dot and Fermi reservoir. Third, the continuous smooth transition in energy from the X^{1-} to the X^0 states signifies the existence of a hybrid exciton (X_H) arising due to strong mixing between the wavefunctions of the discrete quantum dot-states and the continuum of states of the Fermi reservoir[7,25,26]. Fourth, at the crossover point from X^0 to X^{1+} the X^{1+} energetically bends and joins another transition line labelled X_{f+} that arises due to hybridization of the hole with a continuum of states in the Fermi reservoir[27]. Finally, Lorentzian line shapes are observed for the X^0 states far from the hybridization regime, whereas the hybrid and charged excitons exhibit broad and highly asymmetric photoluminescence line shapes with prominent low-energy tails (see Supplementary Fig. 5). These low-energy tails are a consequence of the Anderson orthogonality catastrophe: an energy shakeup process experienced by the electrons in the conduction band (holes in the valence band) when the hybrid excitons recombine and change the electron (hole) level in the quantum dot due to the sudden removal of the intra-quantum-dot Coulomb attraction with the localized hole (electron)[7,28,29]. We apply the Anderson impurity model to extract the tunnel-coupling strength in the device and explain the evolution of each exciton state as a function of V_g. We achieve quantitative agreement with this evolution under the assumption of that the Fermi reservoir is reduced to zero bandwidth at E_F (see Supplementary Equations (1)–(15)). To properly account for the asymmetric photoluminescence line shapes and the continuous transition from X_{f+} to X^{1+}, a more sophisticated calculation involving the density of states in the Fermi reservoir is required[7,27,29]. This calculation and the impact of the Fermi reservoir density of states on the many-body interactions are left for future investigation.

Figure 2d diagrams the initial and final states for the hybridization of the X^0 and X^{1-} states. Filled (open) circles represent electrons (holes), whereas the superscript single (double) arrows account for the possible orientations of the electron (hole) spin. The initial state, composed of two electrons and one hole, is a superposition of different excitonic states: (1) two states that correspond to the quantum dot containing X^0 and an additional electron in the Fermi reservoir, in which the exchange interaction energetically splits the X^0 into two states by Δ_{FSS} $(|QD^{\Uparrow\downarrow}, FR^{\uparrow}\rangle \pm |QD^{\Downarrow\uparrow}, FR^{\downarrow}\rangle)/\sqrt{2}$; and (2) two states that correspond to the excitonic configurations in which the quantum dot has two electrons with opposite spin orientations and a hole ($|QD^{\Uparrow\downarrow\uparrow}\rangle$ and $|QD^{\Downarrow\uparrow\downarrow}\rangle$), giving rise to X^{1-} (with no exchange interaction). After photon emission from the initial state, the final state contains only one electron which is in a superposition of two states: (1) a state corresponding to a linear combination of

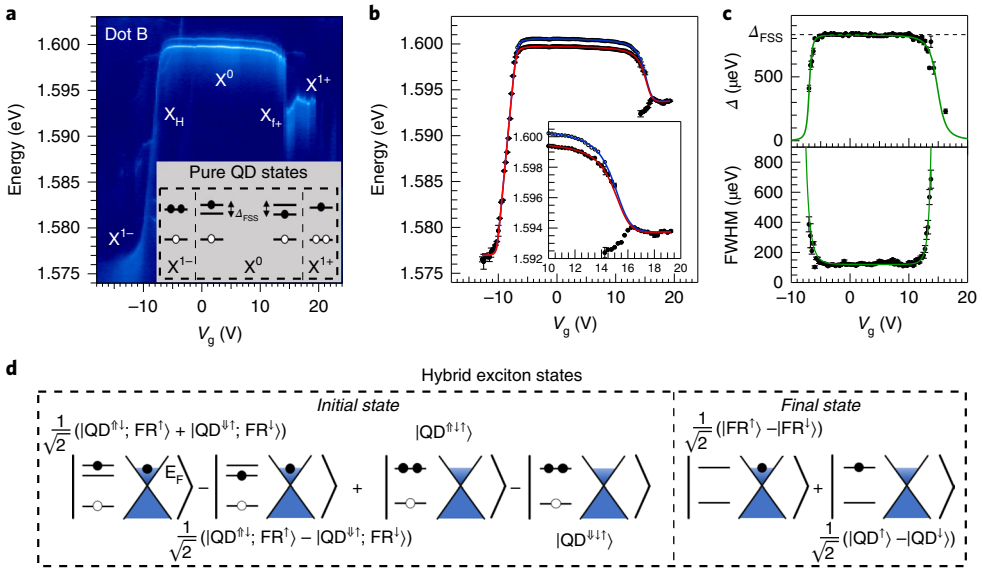

Fig. 2 | Strong tunnel coupling between a quantum dot and a tunable Fermi reservoir in a vdW heterostructure. a, Voltage-dependent high-resolution photoluminescence of dot B. The inset shows a diagram that represents the energy levels of the electrons and the occupation of holes for the pure X^{1-}, X^0 and X^{1+} exciton states of the quantum dot. Δ_{FSS} represents the energy splitting of the fine-structure split X^0 state. **b**, Voltage-dependent evolution of the emission energy for the quantum dot shown in **a**. The solid lines represent fits of the experimental data using the zero-bandwidth model. Details of the theoretical model can be found in Supplementary Equations (1)–(15). The inset displays a zoom of the transition from the X^0 to the X^{1+} exciton state. **c**, Upper panel: experimental (filled circles) and calculated (green line) evolution of the energy splitting (Δ) of the X^0 doublet as a function of V_g. Lower panel: experimental (filled circles) and calculated (green line) voltage-dependent evolution of the photoluminescence linewidth for the low-energy peak of X^0. **d**, Schematic representation of the initial and final states of the X^{1-} to X^0 hybrid exciton. The single (double) arrows represent the spin orientation of a single electron (hole).

the spin orientation states of the remaining electron in the Fermi reservoir ($|FR^{\uparrow}\rangle$ and $|FR^{\downarrow}\rangle$) and (2) a state that is a superposition of the spin orientations for the remaining electron in the quantum dot ($|QD^{\uparrow}\rangle$ and $|QD^{\downarrow}\rangle$). The individual states in both the initial and final state are coupled by a spin-conserving tunnel interaction (see Supplementary Equations (1–15)).

The solid lines in Fig. 2b represent fits of the experimental data to our model, capturing the photoluminescence evolution for both hybrid and bare quantum dot excitons states over the full range of V_g values with high accuracy. The fits reveal an identical lever arm (ratio of device thickness to tunnel barrier thickness) of $\lambda = 145 \pm 10$ for electrons and holes in our device, from which an hBN tunnel barrier thickness of 0.5 ± 0.2 nm (corresponding to one or two monolayers) is obtained. The tunnel-coupling energies for both electrons (V^e_{tun}) and holes (V^h_{tun}) can be directly extracted from the fits; we find $V^e_{tun} = 1.2 \pm 0.2$ and $V^h_{tun} = 3.5 \pm 0.3$ meV. These values are one order of magnitude larger than has been possible in traditional III–V semiconductor devices[7,27]. We attribute the ultra-strong tunnel coupling to the reduction of the tunnel barrier thickness to the atomic layer limit. The ratio $V^h_{tun}/V^e_{tun} = 2.9 \pm 0.5$ is a consequence of the band alignment resulting from the monolayer WSe_2/hBN/graphene heterostructure, which leads to notably lower tunnel barrier heights for holes than for electrons[30]. Using the Wentzel–Kramer–Brillouin approximation for a rectangular tunnelling barrier (see Supplementary Equation (20)), $V^h_{tun}/V^e_{tun} \sim 3.1 \pm 0.4$ can be estimated, in agreement with the experimental result. This approximation can also be employed to explain the tunnel-induced broadening of the photoluminescence linewidth as a function of V_g (see Supplementary Equation (21)), as shown in the bottom panel of Fig. 2c for dot B.

The calculated results in Fig. 2b accurately capture the strong tunnel-induced redshift of the X^0 states at each edge of the X^0 plateau. Different energy shifts are observed for each peak of the doublet, such that the energy splitting of the fine-structure split X^0 excitonic states (Δ) changes as a function of V_g. The top panel of Fig. 2d shows the experimental and calculated evolution of Δ along the X^0 plateau extracted from the data shown in Fig. 2b. In the V_g range corresponding to the pure X^0 quantum dot state $\Delta = \Delta_{FSS}$. However, a fast decrease of Δ is observed near the tunnelling transitions (left and right edges of the X^0 plateau), a consequence of the energy difference that exists between the initial and final hybridized states associated to each of the fine-structure split X^0 states. This is a striking consequence of a large Δ_{FSS} and a strong tunnel coupling: the different eigenstates of X^0 couple differently to the Fermi sea.

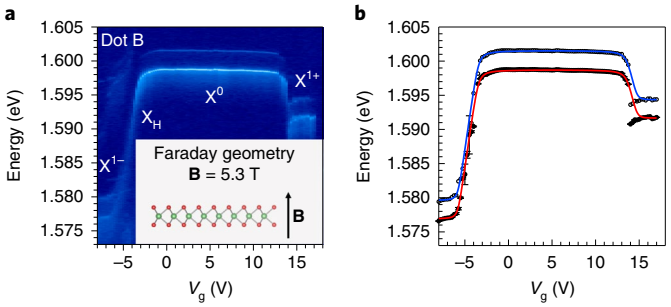

Fig. 3 | Strong tunnel coupling between a quantum dot and a tunable Fermi reservoir at high magnetic field. a, Voltage-dependent high-resolution photoluminescence of dot B for $B_z = 5.3$ T. The inset shows a schematic of the Faraday geometry. **b**, Voltage-dependent evolution of the high-energy (open circles) and low-energy (filled circles) emission peaks extracted from fits of the experimental data shown in **a**. The solid lines represent fits of the experimental data to the zero-bandwidth model described in the Supplementary Equations (16–19).

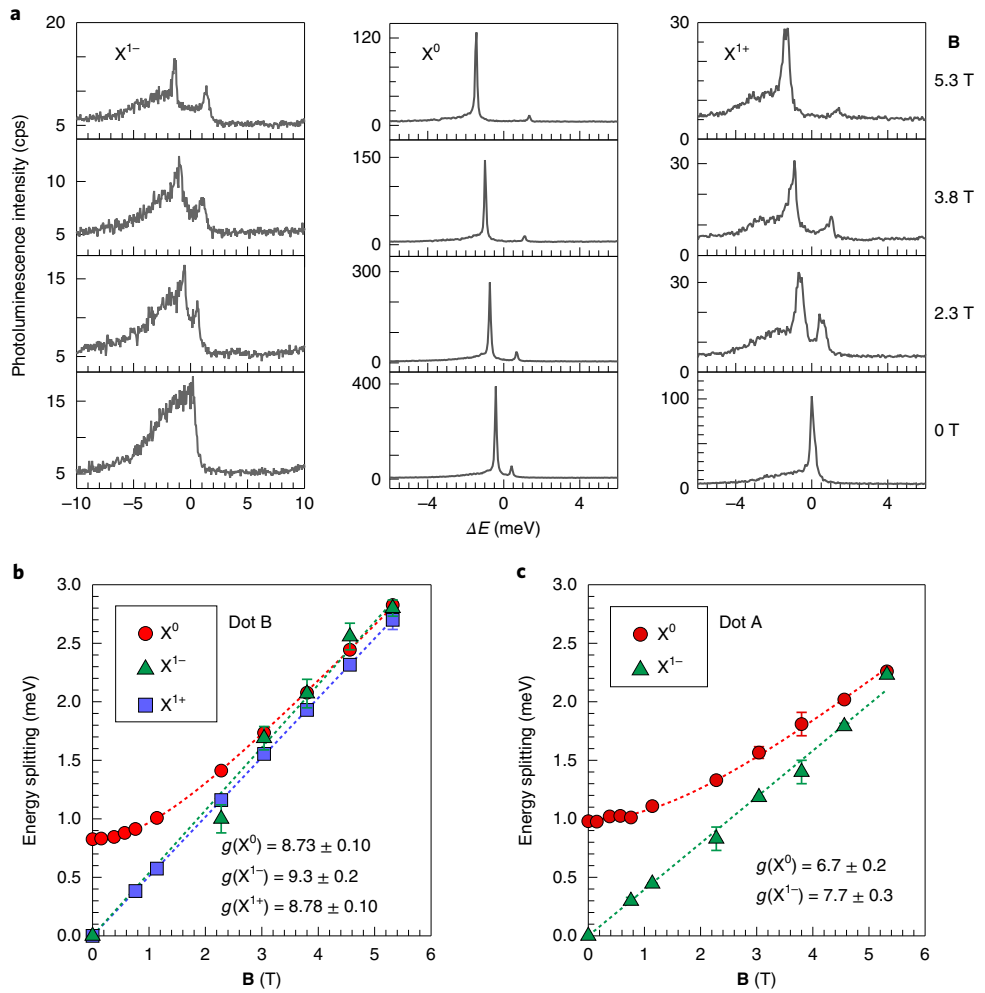

Fig. 4 | Magneto-optics of neutral and charged excitons in WSe_2 quantum dots. a, Photoluminescence spectra of the X^{1-} (left panels), X^0 (central panels) and X^{1+} (right panels) exciton states of dot B under different applied magnetic fields in Faraday geometry. **b**,**c**, Magnetic-field dependence of the energy splitting measured for X^0, X^{1-} and X^{1+} of dot B (**b**) and for X^0 and X^{1-} of dot A (**c**), as obtained from fits of the experimental data shown in **a**. Dashed lines represent fits of the experimental data to Supplementary Equations (22) (X^0) and (23) (X^{1-} and X^{1+}). The fits reveal g values of 8.73 ± 0.10, 9.3 ± 0.2 and 8.78 ± 0.10 for the X^0, X^{1-} and X^{1+} exciton states of dot B, respectively, and g values of 6.7 ± 0.2 and 7.7 ± 0.3 for the X^0 and X^{1-} of dot A, respectively.

The zero-bandwidth model also predicts the existence of the X_{f+} feature in the set of solutions (see Supplementary Equation (14)), although it introduces an artificial splitting between this solution and the experimental result (see Supplementary Fig. 6). Introducing a finite bandwidth for the Fermi reservoir can more accurately model the X_{f+} feature[27] (see Supplementary Fig. 8).

To further investigate the hybridization between the X^0 and X^{1-} and between the X^0 and X^{1+} exciton states, we apply a magnetic field $\mathbf{B}_z$ along the direction perpendicular to heterostructure interfaces (Faraday geometry). Figure 3a shows the result for $\mathbf{B}_z = 5.3$ T; the X^{1-}, X^0 and X^{1+} quantum dot states Zeeman split due to the application of $\mathbf{B}_z$. We adapt our model to explore theoretically the hybridization between exciton states under $\mathbf{B}_z$ (see Supplementary Equations (16–19)). Figure 3b shows the V_g-dependent evolution of the energies for the high- (open circles) and low-energy (filled circles) emission peaks of dot B. The zero-bandwidth model quantitatively reproduces the measured evolution of the photoluminescence energy for ranges of V_g values corresponding to both hybrid and pure quantum dot states. In contrast to the results for $\mathbf{B}_z = 0$ T, the tunnel-induced bending observed at the edges of the X^0 plateau is very similar for both of the fine-structure split X^0 states (Fig. 3a,b) and Δ remains constant. This change in behaviour is a consequence of the reduction in the energy difference between the initial and final hybridized states due to the considerable Zeeman splitting. Notably, these results can only be modelled with spin-conserving tunnelling.

The ability to deterministically load either an electron or hole into the quantum dot allows us to magneto-optically probe the X^{1-} and X^{1+}, respectively, in a WSe_2 quantum dot. Figure 4a shows photoluminescence spectra of the X^{1-} (left panels), X^0 (central panels) and X^{1+} (right panels) exciton states of dot B for varying $\mathbf{B}_z$ values, revealing a clear Zeeman splitting for each state. Figure 4b,c shows the magnetic-field dependence of the energy splitting measured for X^0, X^{1-} and X^{1+} of dot B and for X^0 and X^{1-} of dot A, respectively. The results reveal that the charged excitons exhibit g factors of ~8.7 (dot B) and ~7.7 (dot A), mimicking the behaviour of the corresponding neutral excitons.

Via a Coulomb blockade, we have demonstrated the ability to deterministically load a single electron or single hole in a vdW heterostructure quantum device. This is achieved with gate-tunable tunnel coupling between an optically active WSe_2 quantum dot and a tunable Fermi reservoir in few-layer graphene. Due to an atomically thin tunnel barrier, we obtain ultra-strong and spin-conserving tunnel coupling (roughly one order of magnitude stronger than in conventional III–V quantum devices) between the quantum dot

and Fermi reservoir, leading to the observation of hybrid excitons that can be controlled by the gate voltage. Magneto-optical characterization of the charged excitons reveals large gyromagnetic ratios, indicating that both spin and valley degrees of freedom play an important role for single spins in WSe_2 quantum dots. These results confirm the potential of vdW heterostructures as a new platform for engineering quantum devices. On the one hand, with vdW heterostructures in the strong tunnel-coupling regime, the quantum confined states can be coupled to a tailored or tunable Fermi reservoir. This can enable high-fidelity electrical injection of polarized spins from a nearby ferromagnet or investigation of Kondo-phenomena beyond metallic-like Kondo screening. On the other hand, these results position vdW heterostructures as an intriguing platform to engineer a coherent spin-photon interface. In charge-tunable devices with larger tunnel barriers, a quantum dot can be isolated from its mesoscopic environment. Resonant excitation techniques[1,2,5,31] can then be used to probe and manipulate the valley and spin degrees of freedom and investigate their suitability as coherent quantum bits of information.

Data availability

Data described in this paper are presented in the Supplementary Materials and are available online at https://researchportal.hw.ac.uk/en/persons/brian-d-gerardot.

Received: 8 October 2018; Accepted: 8 February 2019;
Published online: 11 March 2019

References

1. Hanson, R., Kouwenhoven, L. P., Petta, J. R., Tarucha, S. & Vandersypen, L. M. K. Spins in few-electron quantum dots. *Rev. Mod. Phys.* **79**, 1217–1265 (2007).
2. Warburton, R. J. Single spins in self-assembled quantum dots. *Nat. Mater.* **12**, 483–493 (2013).
3. De Franceschi, S. et al. Electron cotunneling in a semiconductor quantum dot. *Phys. Rev. Lett.* **86**, 878–881 (2001).
4. Smith, J. M. et al. Voltage control of the spin dynamics of an exciton in a semiconductor quantum dot. *Phys. Rev. Lett.* **94**, 197402 (2005).
5. Gao, W. B., Imamoglu, A., Bernien, H. & Hanson, R. Coherent manipulation, measurement and entanglement of individual solid-state spins using optical fields. *Nat. Photonics* **9**, 363–373 (2015).
6. Cronenwett, S. M., Oosterkamp, T. H. & Kouwenhoven, L. P. A tunable Kondo effect in quantum dots. *Science* **281**, 540–544 (1998).
7. Latta, C. et al. Quantum quench of Kondo correlations in optical absorption. *Nature* **474**, 627–630 (2011).
8. Kormányos, A., Zólyomi, V., Drummond, N. D. & Burkard, G. Spin–orbit coupling, quantum dots, and qubits in monolayer transition metal dichalcogenides. *Phys. Rev. X* **4**, 011034 (2014).
9. Liu, G. B., Pang, H., Yao, Y. & Yao, W. Intervalley coupling by quantum dot confinement potentials in monolayer transition metal dichalcogenides. *New J. Phys.* **16**, 105011 (2014).
10. Britnell, L. et al. Electron tunneling through ultrathin boron nitride crystalline barriers. *Nano Lett.* **12**, 1707–1710 (2012).
11. Fritz, L. & Vojta, M. The physics of Kondo impurities in graphene. *Rep. Prog. Phys.* **76**, 032501 (2013).
12. Zhang, Z. Z. et al. Electrotunable artificial molecules based on van der Waals heterostructures. *Sci. Adv.* **3**, e1701699 (2017).
13. Wang, K. et al. Electrical control of charged carriers and excitons in atomically thin materials. *Nat. Nanotechnol.* **13**, 128–132 (2018).
14. Srivastava, A. et al. Optically active quantum dots in monolayer WSe_2. *Nat. Nanotechnol.* **10**, 491–496 (2015).
15. He, Y. M. et al. Single quantum emitters in monolayer semiconductors. *Nat. Nanotechnol.* **10**, 497–502 (2015).
16. Tonndorf, P. et al. Single-photon emission from localized excitons in an atomically thin semiconductor. *Optica* **2**, 347–352 (2015).
17. Kumar, S., Kaczmarczyk, A. & Gerardot, B. D. Strain-induced spatial and spectral isolation of quantum emitters in mono- and bilayer WSe_2. *Nano Lett.* **15**, 7567–7573 (2015).
18. Kern, J. et al. Nanoscale positioning of single-photon emitters in atomically thin Wse_2. *Adv. Mat.* **28**, 7101–7105 (2016).
19. Branny, A., Kumar, S., Proux, R. & Gerardot, B. D. Deterministic strain-induced arrays of quantum emitters in a two-dimensional semiconductor. *Nat. Commun.* **8**, 15053 (2017).
20. Palacios-Barraquero, C. et al. Large-scale quantum-emitter arrays in atomically thin semiconductors. *Nat. Commun.* **8**, 15093 (2017).
21. Chakraborty, C. et al. Quantum-confined Stark effect of individual defects in a van der Waals heterostructure. *Nano Lett.* **18**, 2253–2258 (2017).
22. Roch, J. G. et al. Quantum-confined Stark effect in a MoS_2 monolayer van der Waals heterostructure. *Nano Lett.* **18**, 1070–1074 (2018).
23. Chakraborty, C. et al. 3D localized trions in monolayer WSe_2 in a charge tunable van der Waals heterostructure. *Nano Lett.* **18**, 2859–2863 (2018).
24. Bayer, M. et al. Fine structure of neutral and charged excitons in self-assembled In(Ga)As/(Al)GaAs quantum dots. *Phys. Rev. B* **65**, 195315 (2002).
25. Govorov, A. O., Karrai, K. & Warburton, R. J. Kondo excitons in self-assembled quantum dots. *Phys. Rev. B* **67**, 241307(R) (2003).
26. Kleemans, N. A. J. M. et al. Many-body exciton states in self-assembled quantum dots coupled to a Fermi sea. *Nat. Physics* **6**, 534–538 (2010).
27. Dalgarno, P. A. et al. Optically induced hybridization of a quantum dot state with a filled continuum. *Phys. Rev. Lett.* **100**, 176801 (2008).
28. Anderson, P. W. Infrared catastrophe in Fermi gases with local scattering potentials. *Phys. Rev. Lett.* **18**, 1049–1051 (1967).
29. Helmes, R. W., Sindel, M., Borda, L. & von Delft, J. Absorption and emission in quantum dots: Fermi surface effects of Anderson excitons. *Phys. Rev. B* **72**, 125301 (2005).
30. Binder, J. et al. Sub-bandgap voltage electroluminescence and magneto-oscillations in a WSe_2 light-emitting van der Waals heterostructure. *Nano Lett.* **17**, 1425–1430 (2017).
31. Kumar, S. et al. Resonant laser spectroscopy of localized excitons in monolayer WSe_2. *Optica* **3**, 882–886 (2016).

Acknowledgements

This work is supported by the EPSRC (grant nos. EP/L015110/1, EP/P029892/1 and EP/M013472/1) and the ERC (grant nos. 307392 and 725920) and the EU Horizon 2020 research and innovation program under grant agreement no. 820423. Growth of hBN crystals by K.W. and T.T. was supported by the Elemental Strategy Initiative conducted by the MEXT, Japan and the CREST (grant no. JPMJCR15F3), JST. Device fabrication by M.G. and K.S.B. was made possible with support the National Science Foundation, award no. DMR-1709987. B.D.G. is supported by a Wolfson Merit Award from the Royal Society and a Chair in Emerging Technology from the Royal Academy of Engineering.

Author contributions

B.D.G. conceived and supervised the project. A.B. fabricated the samples, assisted by S.K., R. Picard, M.G. and K.S.B. K.W. and T.T. supplied the hBN crystals. M.B.-G. and A.B. performed the experiments, assisted by S.K. and R. Proux. M.B.-G. analysed the data and developed the theoretical model, assisted by B.D.G. M.B.-G. and B.D.G. cowrote the paper with input from all authors.

Competing interests

The authors declare no competing interests.

Additional information

Supplementary information is available for this paper at https://doi.org/10.1038/s41565-019-0402-5.

Reprints and permissions information is available at www.nature.com/reprints.

Correspondence and requests for materials should be addressed to M.B. or B.D.G.

Publisher's note: Springer Nature remains neutral with regard to jurisdictional claims in published maps and institutional affiliations.